Available online at www.sciencedirect.com
SCIENCE DIRECT®
Tetrahedron: Asymmetry
Tetrahedron: *Asymmetry* 16 (2005) 2099–2106

Influence of (*S*)-1-phenylethylamine *para* substitution on the resolution of (±)-1,4-benzodioxane-2-carboxylic acid: a crystallographic, theoretical and morphologic approach

Nicoletta Marchini, Gabriella Bombieri,* Roberto Artali, Cristiano Bolchi, Marco Pallavicini and Ermanno Valoti

Istituto di Chimica Farmaceutica e Tossicologica, Università di Milano, Viale Abruzzi 42, I-20131 Milano, Italy

Received 22 March 2005; accepted 5 May 2005

Abstract—The crystal structures of the salts of (*S*)- and (*R*)-1,4-benzodioxane-2-carboxylic acid with (*S*)-1-phenylethylamine and its *p*-methyl and *p*-nitro substituted analogues were determined in order to correlate the differences in solubility between diastereomeric salts with their solid state structures. A common characteristic of the six structures is the presence of hydrogen bond interactions, which always involve the ammonium group NH_3^+ and the carboxylic oxygens of three adjacent acid molecules with the formation of molecular chains in the direction of the binary screw crystallographic axis (unique axis in the monoclinic system and, in the orthorhombic space group, coincident with the direction of the shortest cell axis). A determinant factor for the high inter diastereomer solubility difference of the two pairs of *p*-methyl and *p*-nitro substituted amine salts seems, in the case of the *p*-methyl derivatives, to be the different mutual disposition of the acid and amine aromatic rings at the boundaries of the molecular chains and, for the *p*-nitro derivatives, the prevalence, in the same region, of the nitro groups or of the acid aromatic moieties. A morphologic study at SEM revealed some correlation between the crystal habit and solubility. Theoretical calculations, based on the LSER model, account for the observed solubilities in methanol.

1. Introduction

The resolution of racemates via diastereomeric salt formation followed by selective crystallization is a well-known and widely practised method for the preparation of enantiopure compounds.[1] In order to identify an efficient resolving agent of (±)-1,4-benzodioxane-2-carboxylic acid (±)-**1**, we have recently[2] investigated the solubilities and melting points of the diastereomeric salts of (*S*)- and (*R*)-**1**, with the *S* forms of 1-phenylethylamine (*S*)-**2**, 1-naphthylethylamine, 2-naphthylethylamine, 1-(4-methylphenyl)ethylamine (*S*)-**3**, 1-(4-nitrophenyl)ethylamine (*S*)-**4** and other *p*-substituted 1-phenylethylamines (*p*-MeO, *p*-Cl, *p*-Br). The large differences between the diastereomeric benzodioxanecarboxylates of (*S*)-**3** and of (*S*)-**4** indicated these latter amines as the best candidates for the resolution of (±)-**1**. Indeed, contrary to (*S*)-**2**, (*S*)-**3** and (*S*)-**4** proved to resolve (±)-**1** with high efficiency. The beneficial influence of the *p*-NO_2 and, unexpectedly, of the *p*-Me substituents prompted us to try to rationalize such results in terms of the possible effects of the crystal packing. Herein, we report the X-ray crystal structures of the three pairs of diastereomeric salts formed by (*S*)-**2**, (*S*)-**3** and (*S*)-**4** with (*S*)- and (*R*)-**1**.

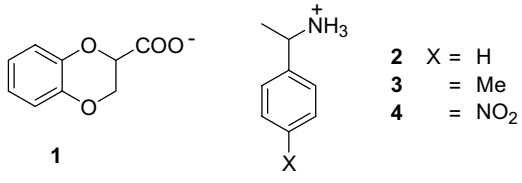

1

Furthermore, considering the different methods reported for solubility prediction[3] (correlations with physico-chemical quantities experimentally determined or based on group contributions and correlations with parameters solely calculated from molecular structure), we used a linear solvation energy relationship (LSER)[4] approach in order to correlate the influence of the crystal structure of the selected salts on the solubility

* Corresponding author. Tel.: +39 02 5031 7516; fax: +39 02 5031 7565; e-mail: gabriella.bombieri@unimi.it

0957-4166/$ - see front matter © 2005 Elsevier Ltd. All rights reserved.
doi:10.1016/j.tetasy.2005.05.010

in methanol. Finally, for some of the same salts, morphologic analysis by SEM is described briefly discussing the correlation of the crystal habit to the salt solubility.

2. Results

2.1. Crystal structures description

A drawing of the molecular structures of the three diastereomeric ion pairs, (*S*)-**2**·(*R*)-**1**, (*S*)-**2**·(*S*)-**1**, (*S*)-**3**·(*R*)-**1**, (*S*)-**3**·(*S*)-**1**, (*S*)-**4**·(*R*)-**1** and (*S*)-**4**·(*S*)-**1**, is shown in Figure 1.

Starting from the structure of (*S*)-**2**·(*R*)-**1** (Fig. 1, top left), we found the presence of two pairs of crystallographic nonequivalent amines and acids. These form salt units, in which the pairs related by a twofold screw axis are the basic molecular skeleton in the formation of independent chains running in the *a*-axis direction (Fig. 2). The two cations (amines) differ in the orientation of the ammonium group, as shown by the torsion

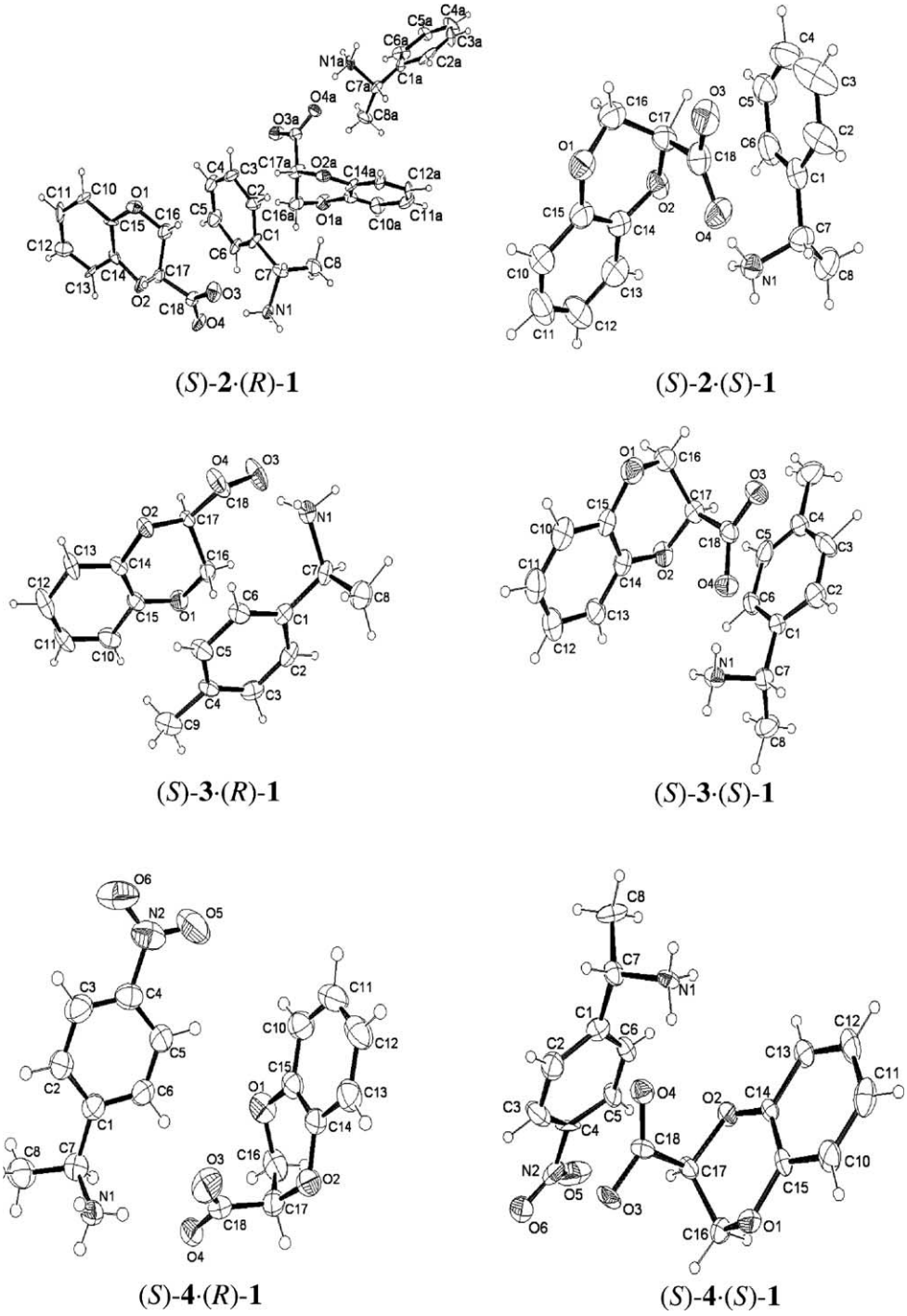

Figure 1. ORTEP[5] views of the independent pairs of the compounds (at 50% probability level). On the left are the more soluble and on the right the less soluble.

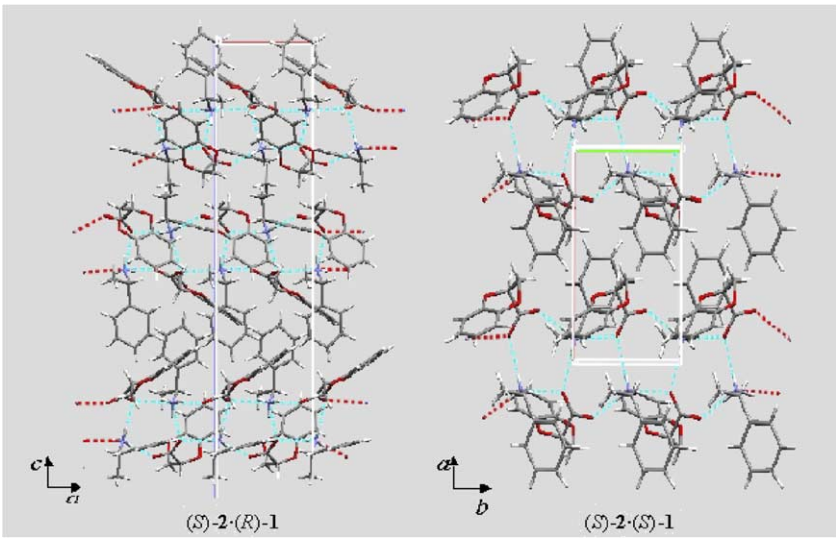

Figure 2. Unit cell content down *b* of (*S*)-**2**·(*R*)-**1** (left) and down *c* of (*S*)-**2**·(*S*)-**1** (right). The hydrogen bonds are given as blue dotted lines, the red ones indicate the chain growing direction as in the following Figures 3 and 4.

angles C6–C1–C7–N1 −37(2)° and C6A–C1A–C7A–N1A −79(2)°, while the two anions (acids) differ in the heterocycle conformation, by the deviations of C16 and C17 from the planar part O1–C15–C14–O2 of 0.24(2) and −0.42(2) Å, respectively, and the corresponding values in the A labelled molecule −0.42(2) and 0.36(2) Å. In the chain organization, one pair is in the upper part of the chain (when considering their representation as shown in Fig. 2, left) while the second pair is in the lower part.

The boundaries of the chain are formed by the methyls on one side and on the other by the amine phenyls, which face to those of the adjacent chains at a 3.5 Å distance, indicative of π interaction.

In (*S*)-**2**·(*S*)-**1**, slightly less soluble than its diastereomer, one pair of amine and acid only forms the basic unit of the crystal (Fig. 1, top right). Compared to (*S*)-**2**·(*R*)-**1**, the amine presents a different orientation of the ammonium with a N1–C7–C6–C1 torsion angle of −60(1)° and the acid slightly differs in conformation with deviations of 0.53(1) Å for C16 and −0.21(1) Å for C17 from the heterocycle plane. The molecular chains are separated only by the amine phenyls (Fig. 2, right).

In the (*S*)-**3**·(*R*)-**1** and (*S*)-**3**·(*S*)-**1** pair (Fig. 1, middle left and right, respectively), the introduction of a methyl substituent onto the *para* position of the amine results in a drastic reduction of solubility of the *SS* form, which becomes about fivefold less soluble than its *SR* diastereomer in methanol. In (*S*)-**3**·(*R*)-**1** (more soluble), the common motif of the columnar molecular assembly along a screw axis is in the direction of the shortest *a*-axis of its orthorhombic cell. The inter chain boundary is characterized by the hydrophobic interactions coming mainly from the *p*-methyls, that are facing each other as shown in Figure 3 (left). The geometrical feature of the amine is quantified by a C6–C1–C7–N1 torsion angle of −35(1)° and, for the acid, by −0.307(9) and 0.396(7) Å

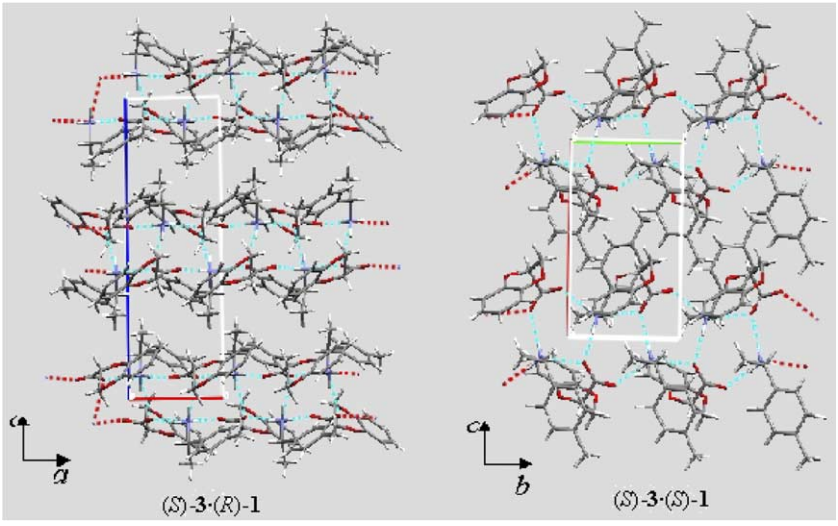

Figure 3. Unit cell content down *b* of (*S*)-**3**·(*R*)-1 (left) and down *a* of (*S*)-**3**·(*S*)-**1** (right).

deviations of C16 and C17 from the heterocycle plane, respectively. A peculiar characteristic is the parallel orientation of the aromatic part of the amine and the acid (the angle between the planes is 4.9(2)°).

In the less soluble (*S*)-**3**·(*S*)-**1**, the orientation of the ammonium is −58.6(7)° (defined by the torsion angle C6–C1–C7–N1), analogously to (*S*)-**2**·(*S*)-**1**. The C16 and C17 positions in the acid are comparable to those of the more soluble diastereomeric salt with deviations of −0.385(8) and 0.365(6) Å from their molecular plane, respectively. The molecular chains are in the direction of the unique *b*-axis of the monoclinic cell. Again, the inter chain boundary is characterized by the hydrophobic interactions coming mainly from the *p*-methyls, which are facing each other as shown in Figure 3 (right). Remarkably, the orientation of the planar aromatic part is no longer parallel.

In the (*S*)-**4**·(*R*)-**1** and (*S*)-**4**·(*S*)-**1** pair, the *p*-methyl substituent of the amine is changed with a *p*-nitro group. In the crystal cell of the more soluble (*S*)-**4**·(*R*)-**1**, such a substitution produces a different ammonium orientation again [torsion angle C6–C1–C7–N1 76.0(2)°], while the nitro group is practically coplanar to the phenyl. The distortion in the hetero cycle is 0.594(2) Å for C16 and −0.101(2) Å for C17. In the crystal packing, the nitro amines are in the external part of the chains and face each other. The molecular chains are in the direction of the crystallographic *a*-axis (Fig. 4, left).

In the less soluble (*S*)-**4**·(*S*)-**1**, the torsion angle C6–C1–C7–N1 is −58(1)° while C16 and C17 are out of the heterocycle plane by −0.49(1) and 0.26(1) Å, respectively. The molecular chains are also in this case in the direction of the *a*-axis but interestingly the external part of the neighbouring chains here is mainly formed by the acids facing each other (Fig. 4, right). In general, the conformation of the arylethylammonium cation is about the same as in the less soluble *SS* salts with a torsion angle C6–C1–C7–N1 ranging between −58° and −60°, while it sensibly varies in the more soluble *SR* salts with values from −37° to −92°.

3. Theoretical investigations

In order to correlate the effect of the crystal structure to the solubility in methanol, a linear solvation energy relationship (LSER) approach was used.[4] The selected descriptors are listed in Table 1, together with the experimental values of $\mathrm{Log_e}\,S$ in methanol[2] (*S* mM).

They include the calculated salt volume (*V*), dipole (*D*), HOMO and LUMO energies (E_{homo} and E_{lumo}, respectively), the N···O distance (Dist, representative of the hydrogen bond interactions) and the COO^- and NH_3^+ partial charges (coded as Q_M and Q_P, respectively). The relationships between the calculated descriptors and $\mathrm{Log_e}\,S_{\mathrm{MeOH}}$ have been analyzed by looking at the correlation matrix values, and all regression equations

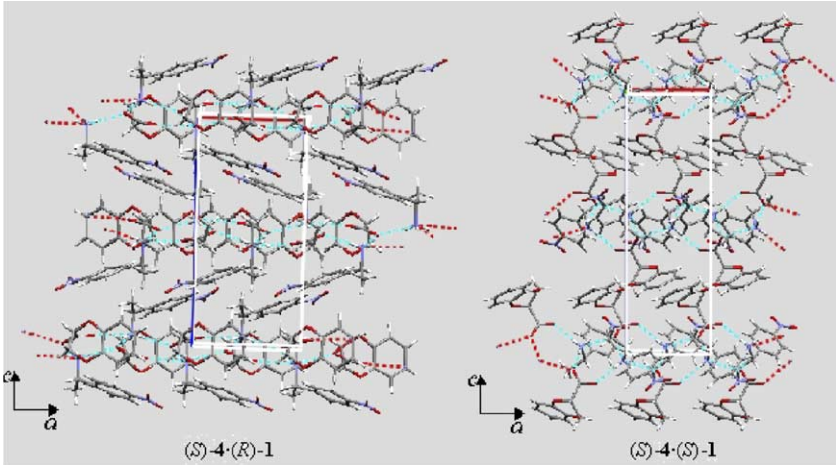

Figure 4. Unit cell content down *b* of (*S*)-**4**·(*R*)-**1** (left) and of (*S*)-**4**·(*S*)-**1** (right).

Table 1. Descriptors for solubility in MeOH

Salts	$\mathrm{Log_e}\,S_{\mathrm{MeOH}}$	Volume (*V*)	Dipole (*D*)	E_{homo}	E_{lumo}	N···O (Dist)	COO^- (Q_M)	NH_3^+ (Q_P)
(*S*)-**2**·(*S*)-**1**	6.00	345.94	10.17	−201.23	−12.99	2.72	−0.31	0.66
(*S*)-**2**·(*R*)-**1**	6.26	346.84	8.87	−195.74	−11.28	2.82	−0.26	0.32
	6.26*	346.33*	9.28*	−192.63*	−19.28*	2.73*	−0.25*	0.30*
(*S*)-**3**·(*S*)-**1**	4.57	365.97	9.99	−200.70	−12.54	2.71	−0.21	0.21
(*S*)-**3**·(*R*)-**1**	6.26	365.66	8.51	−196.46	−10.73	2.90	−0.33	0.42
(*S*)-**4**·(*S*)-**1**	3.26	376.70	11.46	−207.21	−37.67	2.72	−0.33	0.38
(*S*)-**4**·(*R*)-**1**	5.11	375.85	9.39	−199.75	−34.84	2.86	−0.25	0.60
Corr. coefficient	—	−0.75	−0.85	0.87	0.71	0.41	0.33	−0.04
Multiple R^2	—	0.56	0.72	0.76	0.50	0.17	0.11	0.00
Adj. mult. R^2	—	0.48	0.66	0.71	0.40	0.00	−0.07	−0.20

* The asymmetric unit in the crystal cell is formed by two conformationally different molecules.

were evaluated (values reported in Table 1). The analysis of the correlation matrix shows that D and E_{homo} are the best descriptors for $Log_e S_{MeOH}$ (Table 1). The V descriptor was considered because it shows only partial correlations with D and E_{homo} and accounts for steric hindrance of the whole molecule, an effect that could play an important role in the solubility mechanism. This situation was also confirmed by the results of multiple linear regression (MLR) stepwise forward variable selection, while E_{homo} was established as the best single-variable predictor. E_{homo} exhibits the best predictability power, with a partial regression coefficient of 0.87 and an R^2 of 0.76, with respect to $Log_e S_{MeOH}$, leading to the model shown in Eq. 1:

$$\begin{aligned} &Log_e S_{MeOH} = 47.6275 + 0.2121 * E_{homo} \\ &n = 7, \quad R = 0.8706, \quad R^2 = 0.7579, \\ &\text{Adj. } R^2 = 0.7095, \quad p < 0.007 \end{aligned} \tag{1}$$

V, D and Dist appear to improve this equation. However, the best two-variable equation was obtained using E_{homo} and V, although its predictability power is not higher with respect to Eq. 1 with an R^2 of 0.8311.

For the three-terms equation, D and Dist were again selected by the multiple linear regression stepwise forward variable selection to improve the model. The best statistical solution leads to the three-terms Eq. 2 for the solubility in methanol:

$$\begin{aligned} Log S_{MeOH} &= 23.0622 - 0.9244 * D \\ &\quad - 0.0420 * E_{homo} - 0.0475 * V \\ n &= 7, \quad R = 0.9755, \quad R^2 = 0.9517, \\ R^2 \text{ Adj.} &= 0.9033, \quad p < 0.017, \quad \text{SE: } 0.36 \end{aligned} \tag{2}$$

The observed and predicted values, together with the residuals and standard error of the predicted values are shown in Table 2.

A plot of the observed versus predicted $Log_e S_{MeOH}$ solubilities, obtained using the three-term Eq. 2, is shown in Figure 5. The 95% confidence intervals are larger at the extremes than at the centre, and this can be viewed as the uncertainty in defining the slope. Scanning of the residuals (Table 2) shows the absence of real outliers, because the 95% confidence interval includes the observed values, with (*S*)-**2**·(*S*)-**1** and (*S*)-**3**·(*S*)-**1** located at the boundary of the 95% confidence interval (Fig. 5).

The derived LSER model in Eq. 2 adequately accounts for the variations observed in the $Log_e S_{MeOH}$ values for all the examined compounds, providing the solubility values for the two salt conformations in the crystal cell of (*S*)-**2**·(*R*)-**1**. As previously described, the V descriptor in Eq. (2) accounts for the steric effect and, differently from D and E_{homo}, it can also be related directly to the crystal packing. V is an important descriptor in that it explains the variability between the three different substituted amines, but it is unable to give information about the variability inside the diastereoisomeric ion pairs (see Table 1). This kind of information can be obtained by the two other descriptors, D and E_{homo}. E_{homo} can be considered an indicator of the carboxylic group nucleophilic reactivity; it is related to the energy level of the carboxylic acid moiety. The dipole moment D gives instead an idea of the ionic bond strength between the acid/base couple and together with E_{homo} is able to differentiate between *SS* and *SR* diastereomers.

Table 2. Observed and predicted solubility values with residuals and standard errors of the predicted values

	Obs. $Log_e S$	Pred. $Log_e S$	Residuals	Std. pred. val.	Std. err. pred. val.
(*S*)-**2**·(*S*)-**1**	6.00	5.70	0.30	0.28	0.31
(*S*)-**2**·(*R*)-**1**	6.26	6.63	−0.37	1.11	0.23
		6.14*	0.11*	0.68*	0.36*
(*S*)-**3**·(*S*)-**1**	4.57	4.89	−0.32	−0.44	0.15
(*S*)-**3**·(*R*)-**1**	6.26	6.10	0.16	0.64	0.27
(*S*)-**4**·(*S*)-**1**	3.26	3.30	−0.04	−1.86	0.32
(*S*)-**4**·(*R*)-**1**	5.11	4.95	0.16	−0.39	0.24
Min.	3.26	3.30	−0.37	−1.86	0.15
Max.	6.26	6.63	0.30	1.11	0.36
Mean	5.39	5.39	0.00	0.00	0.27

* As in Table 1.

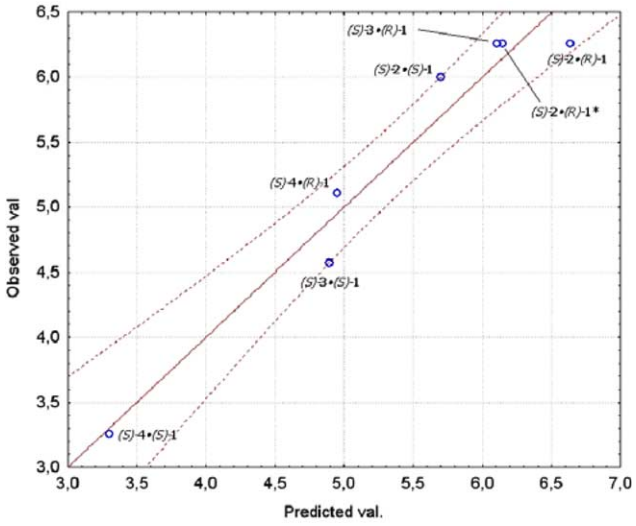

Figure 5. Plot of the predicted versus observed $Log_e S_{MeOH}$ values. The 95% confidence limits are shown as red dashed lines (* as in Table 1).

However, it is important to note that the E_{lumo} energy, which is related to the ammonium group electrophilic reactivity, does not add much more predictability power to the LSER model, indicating a minor importance for the cationic part of the ion pair in the solubility mechanism. In the present case, the $Log_e S_{MeOH}$ was affected not only by the crystal packing (related to the V descriptor), but also by the electronic structure of the whole molecule, indicative of the ability of electron-donating to solvent molecules, and modelled by D and E_{homo}.

The negative values of the coefficients in Eq. 2 show, for the used descriptors, an inverse proportionality with the $Log_e S$ in methanol, particularly for that concerning the

dipole moment *D*, considering this latter as an index of the difficulty in the separation of the carboxylic and ammonium components of the salts.

4. Discussion

The salts are characterized by the presence of molecular chains, where the molecules are connected by intermolecular hydrogen bonds. A common characteristic is that this type of hydrogen bond interaction always involves the ammonium group NH_3^+, which acts as donor with three hydrogen bonds towards the carboxylic oxygens of three adjacent acid molecules. This leads to the formation of molecular chains in the direction of the binary screw crystallographic axis (unique axis in the monoclinic system and, in the orthorhombic space group, coincident with the direction of the shortest cell axis, see Table 3). The cell parameter characterizing the direction of the column varies between 6.6 and 7.3 Å.

The packing of the aromatic moieties has often been indicated as presumably the determinant for the solubility difference between diastereomeric salts. On this basis, we analyzed the orientation of the aromatic groups in the hydrophobic region of the chains (the external part) of the three salt pairs and we found, in the case of the more soluble (*S*)-**3**·(*R*)-**1**, a parallel orientation of the amine and acid aromatic rings, which drastically contrasts with their quasi orthogonal disposition in the less soluble (*S*)-**3**·(*S*)-**1**. In (*S*)-**4**·(*S*)-**1** and (*S*)-**4**·(*R*)-**1**, where the amine is *p*-NO_2 substituted, the respective dihedral angles are about the same in the more and in the less soluble salt being 76.0(4)° and 71.0(4)°, respectively. When the difference in solubility is very low, as in the (*S*)-**2**·(*R*)-**1**/(*S*)-**2**·(*S*)-**1** pair, the situation is more complicated due to the presence, in the crystal cell of the former salt, of two ionic couples slightly differing in conformation. Consequently, two dihedral angle values [19.4(5)° and 49.3(6)°] are observed in (*S*)-**2**·(*R*)-**1**, whereas the same angle is invariably 79.6(4)° in (*S*)-**2**·(*S*)-**1**.

These results could justify the dramatic increase of solubility difference between the *SR* and the *SS* diastereomers associated with the introduction of methyl substituent at the *para* position of (*S*)-**2**. In fact, such a substituent would be responsible for a substantially different disposition of the aromatic moieties in the external part of the chains, efficiently herring-bone packed in (*S*)-**3**·(*S*)-**1** and instead parallel in its much more soluble (*S*)-**3**·(*R*)-**1** diastereomer. Consistently with this hypothesis, the negligible solubility difference between the two diastereomeric salts of (*S*)-**2** should not be interpreted in terms of higher solubility of (*S*)-**2**·(*S*)-**1**, that shows a quasi orthogonal disposition of the aromatic moieties such as in (*S*)-**3**·(*S*)-**1**, but rather of relatively low solubility of (*S*)-**2**·(*R*)-**1**, somehow related to the exceptional presence of two conformationally different ionic couples in the basic salt units of (*S*)-**2**·(*R*)-**1**. This hypothesis can also be confirmed by the results based on Eq. 2, where the two crystallographically independent molecules show different solubilities, respectively, lower and higher, with respect to the observed one. The same analysis indicates that the solubility difference between diastereomers produced by the *p*-NO_2 substituent, comparable to that induced by *p*-Me, could not be related only to the reciprocal orientation of the aromatic moieties, which is about the same in (*S*)-**4**·(*S*)-**1** and (*S*)-**4**·(*R*)-**1**, but tentatively identified with the prevalence of the polar *p*-nitrophenyl residues at the chain boundaries of the more soluble (*S*)-**4**·(*R*)-**1** in contrast with that of the apolar acid aromatic portions in the less soluble (*S*)-**4**·(*S*)-**1**.

At this point, we thought it useful to consider other parameters such as the strength of the hydrogen bonds involved in the molecular chain formation. However, a detailed analysis of the intra chain hydrogen bond geometries did not highlight significant correlations with the diastereomer difference in solubility. With respect to this, an analysis of the inter chain interactions in terms of C–H···O distances, where the carbon is part of an aromatic system, was not completely developed.

The trend of the solubility values in methanol was correctly predicted using a linear solvation energy relationship (LSER) approach. In particular, the best predictability power of the HOMO energy parameter, indicative of the carboxylic group nucleophilic reactivity, was disclosed.

We also considered the morphologic aspect of the salts in the solid state by scanning electron microscopy (SEM) in order to find additional correlations between the crystal shape and solubility.

We found that the SEM images of the differently soluble salts are also morphologically different (Fig. 6). The crystals are thinner and the 'lamellar' structure is in favour of a bigger flaking for the more soluble ones, while

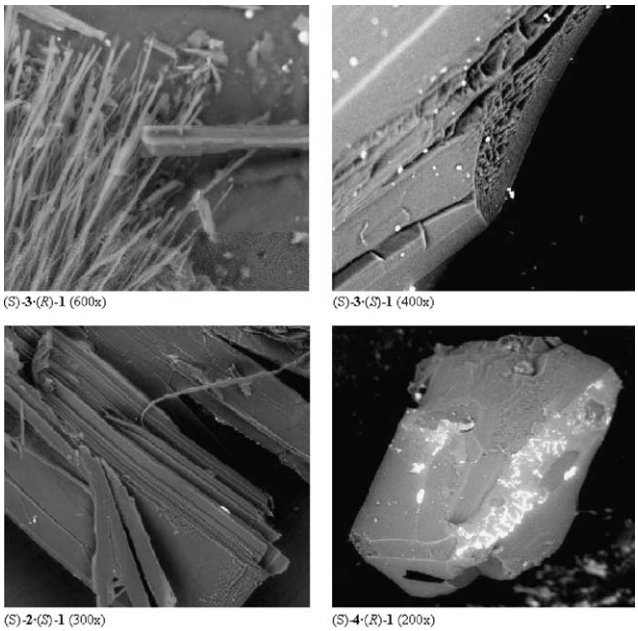

Figure 6. SEM images.

the lower solubility is associated with more compact structures, as shown in Figure 6 for the (*S*)-**3**·(*R*)-**1**/(*S*)-**3**·(*S*)-**1** pair (top). For the salts of the unsubstituted amine, we have the image only of the (*S*)-**2**·(*S*)-**1** isomer (bottom left), whose solubility is comparable with that of the (*S*)-**3**·(*R*)-**1** isomer, showing the lamellar habit characteristic of soluble compounds. The nitro salt (*S*)-**4**·(*R*)-**1** (bottom right) has the compact structure typical for poorly soluble compounds.

5. Conclusion

The crystallographic investigation of the present diastereomeric salt pairs allows some observations to be made, as we had the opportunity to determine the crystal structures of both diastereomers and to compare them. The importance of the hydrogen bond in the construction of the molecular chains present in all the examined compounds was recognized, but the correlation between NH donor–O acceptor distances and the inter diastereomer solubility differences was questionable as well as the correlation with the C–H···O inter chain interactions. As expected, these solubility differences, arising from the introduction of two very different substituents, NO_2 and CH_3, into the *para* position of 1-phenylethylamine, could not be associated with a common effect of the ring substituent. In fact upon inspection of the structures of the two diastereomeric *p*-methylphenylethylamine benzodioxanecarboxylates it was seen that a different mutual disposition of the amine and acid aromatic rings mainly distinguishes the two salts. Otherwise, no discrimination can be made, on this basis, between the two diastereomeric *p*-nitrophenylethylamine benzodioxanecarboxylates, which instead differentiate for the prevalence of the *p*-nitro substituent or of the acid aromatic portion at the chain boundaries. Therefore, the high solubility differences between the *SS* and the respective *SR* isomers of the two pairs of *p*-substituted phenylethylamine diastereomeric salts could be reasonably linked with these two kinds of structural differences.

In methanol, the solubility trend of the three pairs of salts agrees with the theoretical computation based on LSER approach, highlighting an interestingly significant correlation with the HOMO energy parameter. Finally, the morphologic aspect of the salts (SEM images) is consistent with the observed solubility behaviours.

From this analysis, it appears that more factors play an important role for the diastereo-discrimination upon crystallization and the introduction of heterogeneous substituents can unpredictably produce, inside a congeneric structure series, distinct inter diastereomer differences in the crystal packing, anyhow resulting in similar inter diastereomer differences in solubility.

6. Experimental

6.1. Crystal structure determination and refinement

The crystals of $C_{17}H_{19}N_1O_4$ (*S*)-**2**·(*R*)-**1**, (*S*)-**2**·(*S*)-**1** and of $C_{18}H_{21}N_1O_4$ (*S*)-**3**·(*R*)-**1**, (*S*)-**3**·(*S*)-**1** were obtained from methanol and $C_{17}H_{19}N_2O_6$ (*S*)-**4**·(*R*)-**1**, (*S*)-**4**·(*S*)-**1** from methanol and water (2:1) as colourless prisms. A summary of the crystal data, data collection and structure refinement is presented in Table 3. The intensity data were collected with a CAD4 diffractometer with graphite monochromated MoKα radiation (λ 0.71073 Å). The cell parameters were determined and refined by least-squares fit of 20 high angle reflections. The structures were solved by direct methods[6] and

Table 3. Crystal data and structure refinement of the salts (*S*)-**2**·(*R*)-**1**, (*S*)-**2**·(*S*)-**1**, (*S*)-**3**·(*R*)-**1**, (*S*)-**3**·(*S*)-**1** (*S*)-**4**·(*R*)-**1**, (*S*)-**4**·(*S*)-**1**

Compound	(*S*)-**2**·(*R*)-**1**	(*S*)-**2**·(*S*)-**1**	(*S*)-**3**·(*R*)-**1**	(*S*)-**3**·(*S*)-**1**	(*S*)-**4**·(*R*)-**1**	(*S*)-**4**·(*S*)-**1**
Empiric formula	$C_{17}H_{19}NO_4$	$C_{17}H_{19}NO_4$	$C_{18}H_{21}NO_4$	$C_{18}H_{21}NO_4$	$C_{17}H_{19}N_2O_6$	$C_{17}H_{19}N_2O_6$
FW	301.33	301.33	315.36	315.36	346.33	346.33
Crystal syst.	Orthorhombic	Monoclinic	Orthorhombic	Monoclinic	Orthorhombic	Orthorhombic
Space group	$P2_12_12_1$	$P2_1$	$P2_12_12_1$	$P2_1$	$P2_12_12_1$	$P2_12_12_1$
Unit cell (Å)	a = 6.738(7)	a = 11.028(3)	a = 6.636(2)	a = 11.553(9)	a = 7.3260(10)	a = 6.595(8)
	b = 12.246(8)	b = 6.752(6)	b = 14.943(4)	b = 6.630(6)	b = 14.373(5)	b = 13.544(9)
	c = 38.507(9)	c = 11.706(6)	c = 16.984(2)	c = 11.660(7)	c = 15.697(3)	c = 18.766(9)
		β = 111.50(5)°		β = 108.71(5)°		
Volume (Å^3)	3177.4(12)	811.0(9)	1684.2(7)	845.9(11)	1652.8(11)	1676(2)
Z	8	2	4	2	4	4
Calcd density (Mg/m^3)	1.260	1.234	1.244	1.238	1.396	1.372
Abs. coeff. (mm^{-1})	0.090	0.088	0.088	0.087	0.107	0.105
F(000)	1280	320	672	336	732	732
Crystal size (mm)	0.06 × 0.07 × 0.1	0.11 × 0.16 × 0.09	0.09 × 0.12 × 0.08	0.05 × 0.07 × 0.08	0.11 × 0.09 × 0.13	0.07 × 0.06 × 0.08
θ Range (°)	2.1–17.5	2.2–22.0	2.4–20.0	2.2–22.0	2.6–25.0	2.2–22.0
Limiting indices	$-1 \leqslant h \leqslant 5$	$-11 \leqslant h \leqslant 11$	$-1 \leqslant h \leqslant 6$	$-12 \leqslant h \leqslant 1$	$-8 \leqslant h \leqslant 8$	$-6 \leqslant h \leqslant 6$
	$-1 \leqslant k \leqslant 10$	$-6 \leqslant k \leqslant 1$	$-1 \leqslant k \leqslant 14$	$-6 \leqslant k \leqslant 1$	$-1 \leqslant k \leqslant 17$	$-1 \leqslant k \leqslant 14$
	$0 \leqslant l \leqslant 32$	$-12 \leqslant l \leqslant 1$	$-1 \leqslant l \leqslant 16$	$-11 \leqslant l \leqslant 12$	$-1 \leqslant 1 \leqslant 18$	$-1 \leqslant l \leqslant 19$
Ref. coll./uniq.	1704/1564	1517/1299	981/947	1588/1355	3647/2907	2578/2034
Refinement method	Full-matrix least-squares on F^2					
Data/param.	1564/401	1299/244	947/277	1355/277	2907/298	2034/256
Goodness of fit on F^2	1.09	1.21	1.07	1.02	1.11	0.97
Final R [$I > 2\sigma(I)$]	0.072	0.054	0.034	0.039	0.037	0.052
$wR2$	0.204	0.162	0.085	0.095	0.089	0.107

conventional Fourier synthesis. The refinement of the structures was made by full matrix least-squares[7] on F^2. All non-H-atoms were refined anisotropically. The H-atoms' positions were detected in a difference Fourier synthesis and refined with isotropic thermal factors, or introduced in calculated positions in their described geometries and allowed to ride on the attached carbon atom with fixed isotropic thermal parameters ($1.2U_{eq}$ of the parent carbon atom). The supplementary crystallographic data have been deposited with the Cambridge Crystallographic Data Centre (CCDC deposition numbers 265411, 265412, 265413, 265414, 265415 and 265416. Copies can be obtained, free of charge, from CCDC, 12 Union Road, Cambridge CB2 1EZ, UK; fax: +44(1223) 336033; e-mail: deposit@ccdc.cam.ac.uk).

6.2. Computational methods

Atomic positions as obtained from the crystallographic analysis were used for the theoretical descriptor calculations. In particular, the X-ray conformations were subjected to single point energy calculation, at the DFT levels of theory, using the 6-31+G(d,p)[8] basis set. All the calculations were carried out using the Becke's three-parameter hybrid functional with gradient corrections provided by the LYP functional (B3LYP).[9] The energies were corrected by thermal and entropic (298 K) effects using the standard procedures in GAUSSIAN-03.[10] In the SCRF calculations the solvent effects were incorporated. The coefficients in Eq. 1 were obtained through multiple linear regression (MLR) using home built-in routines, written in SCILAB 2.7.[11] The variables have been selected by using the stepwise approach.

Acknowledgements

We are indebted to the Ministero dell'Istruzione dell'Università e della Ricerca of Italy for financial support. We acknowledge particularly Goffredo Alfieri (Bracco Imaging, CRM, Milano, Italy) for the SEM images and Bracco Imaging for a grant to R.A.

References

1. Jacques, J.; Collet, A.; Wilen, S. H. *Racemates and Resolutions*; Krieger Publishing Company: Malabar, FL, 1994.
2. Bolchi, C.; Pallavicini, M.; Fumagalli, L.; Marchini, N.; Moroni, B.; Rusconi, C.; Valoti, E. *Tetrahedron: Asymmetry* **2005**, *16*, 1639.
3. Yalkowsky, S. H.; Banerjee, S. *Aqueous Solubility: Methods of Estimation for Organic Compounds*; Dekker: New York, 1992.
4. Farah, J. P. S.; Lima, G. A. R.; Quina, F. H. *J. Mol. Struct. (Theochem)* **1997**, *394*, 267.
5. Johnson, C. K.; ORTEP 11, Report ORNL-5138, Oak Ridge National Laboratory, TN, 1976.
6. Altomare, A.; Burla, M. C.; Camalli, M.; Cascarano, G.; Giacovazzo, C.; Gagliardi, A.; Polidori, G. *J. Appl. Crystallogr.* **1994**, *27*, 435.
7. Sheldrick, G. M. SHELX-97, University of Göttingen, Germany.
8. Frisch, M. J.; Pople, J. A.; Binkley, J. S. *J. Chem. Phys.* **1984**, *80*, 3265.
9. Becke, A. D. *J. Chem. Phys.* **1993**, *98*, 1372; Stephens, P. J.; Devlin, F. J.; Chabalowski, C. F.; Frisch, M. J. *J. Phys. Chem.* **1994**, *98*, 1623.
10. Frisch, M. J.; Trucks, G. W.; Schlegel, H. B.; Scuseria, G. E.; Robb, M. A.; Cheeseman, J. R.; Montgomery, J. A., Jr.; Vreven, T.; Kudin, K. N.; Burant, J. C.; Millam, J. M.; Iyengar, S. S.; Tomasi, J.; Barone, V.; Mennucci, B.; Cossi, M.; Scalmani, G.; Rega, N.; Petersson, G. A.; Nakatsuji, H.; Hada, M.; Ehara, M.; Toyota, K.; Fukuda, R.; Hasegawa, J.; Ishida, M.; Nakajima, T.; Honda, Y.; Kitao, O.; Nakai, H.; Klene, M.; Li, X.; Knox, J. E.; Hratchian, H. P.; Cross, J. B.; Bakken, V.; Adamo, C.; Jaramillo, J.; Gomperts, R.; Stratmann, R. E.; Yazyev, O.; Austin, A. J.; Cammi, R.; Pomelli, C.; Ochterski, J. W.; Ayala, P. Y.; Morokuma, K.; Voth, G. A.; Salvador, P.; Dannenberg, J. J.; Zakrzewski, V. G.; Dapprich, S.; Daniels, A. D.; Strain, M. C.; Farkas, O.; Malick, D. K.; Rabuck, A. D.; Raghavachari, K.; Foresman, J. B.; Ortiz, J. V.; Cui, Q.; Baboul, A. G.; Clifford, S.; Cioslowski, J.; Stefanov, B. B.; Liu, G.; Liashenko, A.; Piskorz, P.; Komaromi, I.; Martin, R. L.; Fox, D. J.; Keith, T.; Al-Laham, M. A.; Peng, C. Y.; Nanayakkara, A.; Challacombe, M.; Gill, P. M. W.; Johnson, B.; Chen, W.; Wong, M. W.; Gonzalez, C.; Pople, J. A. *Gaussian 03, Revision C.02*; Gaussian: Wallingford, CT, 2004.
11. Scilab 2.7, http://scilabsoft.inria.fr/.